Topologically nontrivial electronic states in $CaSn_3$

Cite as: J. Appl. Phys. **121**, 214901 (2017); https://doi.org/10.1063/1.4984262
Submitted: 27 March 2017 . Accepted: 15 May 2017 . Published Online: 01 June 2017

Sunny Gupta, Rinkle Juneja, Ravindra Shinde, and Abhishek K. Singh

Topologically nontrivial electronic states in $CaSn_3$

Sunny Gupta, Rinkle Juneja, Ravindra Shinde, and Abhishek K. Singh[a)]
Materials Research Center, Indian Institute of Science, Bangalore 560012, India

(Received 27 March 2017; accepted 15 May 2017; published online 1 June 2017)

Based on the first-principles calculations, we theoretically propose topologically non-trivial states in a recently experimentally discovered superconducting material $CaSn_3$. When the spin-orbit coupling (SOC) is ignored, the material is a host to three-dimensional topological nodal-line semimetal states. Drumhead like surface states protected by the coexistence of time-reversal and mirror symmetry emerge within the two-dimensional regions of the surface Brillouin zone connecting the nodal lines. When SOC is included, unexpectedly, each nodal line evolves into two Weyl nodes (W1 and W2) in this centrosymmetric material. Berry curvature calculations show that these nodes occur in a pair and act as either a source or a sink of Berry flux. This material also has unique surface states in the form of Fermi arcs, which unlike other known Weyl semimetals forms closed loops of surface states on the Fermi surface. Our theoretical realization of topologically non-trivial states in a superconducting material paves the way towards unraveling the interconnection between topological physics and superconductivity. *Published by AIP Publishing.*
[http://dx.doi.org/10.1063/1.4984262]

I. INTRODUCTION

Topological insulators with their non-trivial band topologies exhibiting symmetry protected metallic edge/surface states in insulating bulk 2D/3D materials have attracted widespread interest in recent times.[1,2] Furthermore, the discovery of these unique non-trivial band topologies in semimetals and metals has significantly expanded the family of topological materials much beyond topological insulators.[3–12] These topological semimetallic/metallic (TSM) materials have unique Fermi surfaces ranging from 0D (points) and 1D (lines/loops) to 2D (planes). To date, four types of topological semimetals/metals have been proposed: (i) 3D Dirac Semimetal (DSM), where 4-fold degenerate bands touch close to the Fermi level, with their low energy excitations as Dirac fermions, (ii) Weyl Semimetal (WSM), where 2-fold bands touch in the close vicinity of the Fermi level giving gapless nodes [Weyl Point (WP)], which always comes in pairs of opposite chirality acting as either a source or a sink of the Berry curvature, (iii) topological nodal line semimetal/metal (TNLSM), where band touching (BT) occurs along one-dimensional curves (lines/loops) in k space of materials, and (iv) topological materials beyond Dirac and Weyl fermions, where linear and quadratic three-, six-, and eight-band crossings are stabilized by space group symmetries with spin-orbit coupling (SOC) and time-reversal symmetries.[13–15] The presence of these unique band topologies in TSM materials is constrained by crystallographic symmetries and provides new opportunities for exploring exotic topological physics. The distant topological features of these materials are directly reflected in their peculiar electronic/magnetic properties such as large magnetoresistance and ultrahigh mobility,[10,11,16] chiral anomaly and negative magnetoresistance,[17–19] and Aharonov-Bohm oscillations.[20]

Apart from widespread potential applications of these topological materials, the research on the topological quantum matter has garnered much attention due to its intimate connection to high energy physics, by the introduction of Dirac, Weyl, and Majorana fermions (MFs) into the electronic spectra of crystals. Dirac and Weyl's fermionic systems have been realized experimentally; however, experimental realization of MFs is still a challenge. The MFs are predicted to emerge in the topological superconductor, and introducing superconductivity into the topological materials can serve as a host for these fermionic particles.[1,2,21–24] Superconductivity has been observed in some topological materials with doping[25–27] and external applied pressure.[28] However, an intrinsic superconducting topological material has not been discovered yet. A discovery of an intrinsic superconducting topological material is of utmost importance, and a realization of the same will help in providing more insights into MFs and applications in the future quantum technologies.[29]

Here, using the first-principles density functional theory (DFT) calculations, we have studied the electronic properties of a recently discovered superconducting material $CaSn_3$ with a measured $T_c \approx 4.2$K.[30] This material is found to be a topological nodal line semimetal with drumhead surface states in the absence of spin-orbit coupling (SOC). The bands touch along a line in a large energy window of $\sim(-0.5$–$1.8)$ eV. Moreover, this material unexpectedly turns into a Weyl semimetal with the inclusion of SOC. The Weyl nodes W1 and W2 are found to occur at $k(\frac{2\pi}{a}) = (0.2, 0.2, 0.2)$ and $(0.167, 0.167, 0.167)$, respectively. The Weyl points act like "magnetic" monopoles in momentum space with a charge given by their chirality. They are either a source or a sink of "Berry flux," which is confirmed by Berry curvature calculations. A total of 8 pairs of WPs were identified in the Brillouin zone. We also observed the clear Fermi arcs connecting the Weyl nodes in the surface state calculations. This behavior is similar to the many other topological materials,[6]

a)Electronic mail: abhishek@mrc.iisc.ernet.in

where the WSM phase appears from nodal rings on an inclusion of SOC. Thus, in principle, on tuning the SOC strength, one can achieve a transition between the two topological phases. Our prediction of topological states in a superconducting material $CaSn_3$ provides a promising platform for realizing a topologically superconducting material and the synergy between topological physics and superconductivity.

II. METHODOLOGY

Theoretical calculations were performed within the first-principles density functional theory (DFT)[31] using the Vienna *Ab initio* Simulation Package (VASP).[32,33] Ion-electron interactions were represented by all-electron projector augmented wave potentials.[34,35] The Perdew-Burke-Ernzerhof[36] generalized gradient approximation (GGA) was used to account for the electronic exchange and correlation. The wave functions were expanded in a plane wave with a high energy cut-off of 500 eV and a Monkhorst-Pack[37] **k**-grid of $15 \times 15 \times 15$. The structure was fully relaxed by employing a conjugate gradient scheme until the Hellmann-Feynman forces on the atoms were less than 0.001 eV/Å. Electronic structure calculations were done both with and without SOC. The Berry curvature was calculated using the maximally localized Wannier functions (MLWFs) as implemented in the Wannier90.[38] The surface spectrum including the surface projected band structure and the Fermi surface was calculated based on the iterative Green's function method[39] after obtaining the tight-binding Hamiltonian from the MLWF[38] as implemented in the WannierTools software.[40]

III. RESULTS AND DISCUSSION

$CaSn_3$ crystallizes in a cubic $AuCu_3$ type structure with space group $Pm\bar{3}m$.[30] Ca forms a simple cubic lattice with Sn atoms octahedrally coordinated to each other with no atoms in the center, as shown in Fig. 1(a). The lattice constant $a = 4.74$ Å was taken from a recent experimental report on $CaSn_3$.[30] The ions were then relaxed fixing the volume as well as the lattice constant of the unit cell.

We first study the electronic structure of $CaSn_3$ in the absence of SOC. The band structure along high symmetry lines is shown in Fig. 2(a). The valence (N) band and conduction (N + 1) band have been distinguished with different colors, where N is the total number of valence electrons. It can be seen that there is a band touching (BT) close to the Fermi line along the X-M direction as well as the X-R direction between N and N + 1 bands. To check the orbital character of the bands at these special points as well as at other points along the high symmetry lines, we plotted the orbital decomposed band structure as shown in Fig. 2(b). Only Sn s and p_x orbital contribution has been shown because of their dominance near the Fermi level. The contribution of s and p_x character is mixed near the BT points; however, a clear band inversion can be seen at the M point, indicating possible nontrivial band topologies. The valence band near the Fermi level has s character, while the conduction band has p_x character. This is opposite to the natural order of band filling and clearly signifies a band inversion. The band inversion at the M point is not due to SOC. Such a peculiar band inversion has also been observed in topological nodal line semimetals [AX_2 (A = Ca, Sr, Ba; X = Si, Ge, Sn)[41] and Cu_3PdN[42]] and a topological semimetal (KNa_2Bi),[43] indicating the presence of either reflection or other point group symmetries in the case of noncentrosymmetric or centrosymmetric materials, respectively.[44]

An interesting band topology is exemplified in the band structure of $CaSn_3$. The N and N + 1 bands overlap between a portion of the R-Γ direction. The overlap ranges from ~1.8 eV above the Fermi energy (E_F) to ~0.5 eV below E_F [Fig. 2(a)]. On plotting the band structure along a symmetry direction perpendicular to the R-Γ direction, we see linearly dispersing Dirac cones near the BT points [Fig. 2(d)]. These Dirac cones persist over the R-Γ direction from $k(\frac{2\pi}{a}) = (0.225, 0.225, 0.225) \rightarrow (0.035, 0.035, 0.035)$, signifying the material to be a topological nodal line semimetal. The special symmetries of the crystal present plays an important role in deciding the topological protections of nodal lines in a material. It has been proposed that a material should possess either a product of a mirror and time-reversal symmetry or reflection symmetry for the topological protection of nodal lines.[44,45] In $CaSn_3$, the topological nodal lines are robust and topologically protected because of the coexistence of both time-reversal and mirror symmetry in the

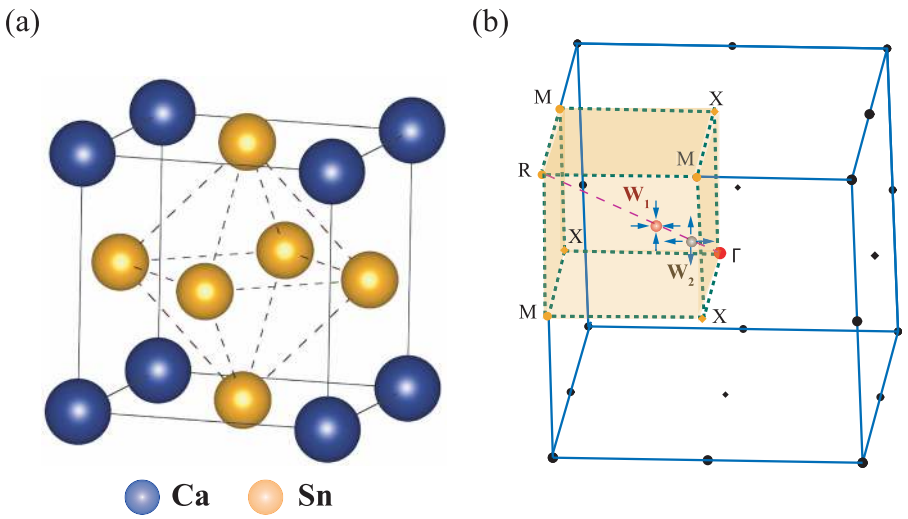

FIG. 1. (a) Crystal structure of $CaSn_3$ and (b) Brillouin zone of $CaSn_3$, showing the high symmetry points as well as the location of Weyl nodes (W_1 and W_2). The Weyl nodes act as either a sink (W_1) or a source (W_2) of the Berry curvature.

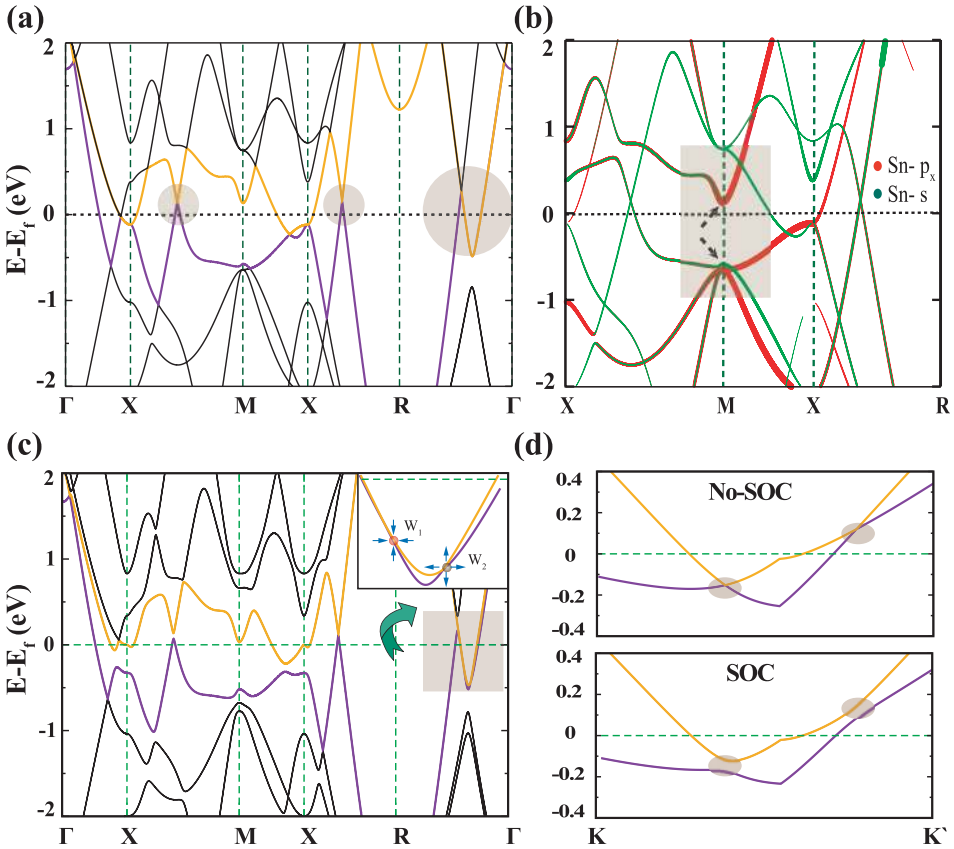

FIG. 2. (a) Bulk band structure of $CaSn_3$ without spin-orbit coupling (SOC). The shaded area depicts the band touching/overlapping regions. (b) Orbital decomposed band structure of $CaSn_3$, showing the contribution of Sn s and p_x orbitals. The shaded area at the M point depicts the band inversion region. (c) Bulk band structure of $CaSn_3$ with SOC. The inset shows the magnified region where the overlapping bands split into two Weyl nodes (W_1 and W_2). The arrows around the Weyl nodes depict the sign of the calculated Berry curvature. (d) Band structure of $CaSn_3$ along a line perpendicular to the R-Γ direction, showing band touching Dirac cones along the nodal line both with and without SOC.

crystal. Due to the special point group symmetry of the crystal, a total of eight nodal lines occur between R-Γ in the 3D Brillouin zone of $CaSn_3$. In this material, being a metal, the crossings between bands other than N and N + 1 are very important. However, in this case, they at much higher/lower energies to be of any practical significance.

The surface states in topological materials are usually related to a topological invariant given by the Berry phase, and a non-zero value guarantees the existence of the topological surface state. In topological nodal line semimetals, it has been shown that the Berry phase is non-zero for any closed path joining the nodal lines.[44,46,47] This implies that the surface states occur within the two-dimensional regions of the surface Brillouin zone connecting the nodal lines. These surface states have a peculiar feature of a "drumhead" when projected on a 2D plane and a surface flat band when viewed along a 1D line.[9,41,45] Thus, to probe the existence of these peculiar surface states, we calculated the surface projected band structure and the Fermi surface on a semi-infinite (001) surface [see Figs. 3(a) and 3(b)], using the iterative Green's function method[39] as implemented in WannierTools.[40] The white and light-blue regions represent the spectral weight of some additional bulk bands near the surface region, whereas the dark blue curves show the surface states. The Dirac cone arising from the bulk states is observed on both the bottom and top surface along the high symmetry direction X-M-Y. Moreover, there exist surface flat bands connecting the two Dirac cones inside the nodal line ring, namely, the "drumhead" states. The surface bands are not flat, as reported in the literature,[42,45] and are dispersive. The dispersive nature of these drumhead states arises because of the nodal line not being at the same energy level due to the particle-hole asymmetry.[9,42,45] These surface flat bands should be directly reflected in the drumhead surface states. Thus, to visualize these drumhead states, we calculated the Fermi surface of the (001) surface [Fig. 3(c)]. The states were calculated at a chemical potential of −0.1 eV. A prominent "drumhead" surface state can be clearly seen in the Fermi surface plot, Fig. 3(c), signifying the existence of topological nodal lines.

In the presence of SOC, the nodal lines are expected to undergo a transition to different topological phases. In many 3D systems, SOC splits the BT points and creates a gap leading to a topological insulator.[48] Also, if some special symmetries are present, nodal line semimetals will persist even in the presence of SOC.[46] However, in $CaSn_3$ with SOC, the nodal lines evolve into a pair of Weyl nodes although the material preserves inversion and time-reversal symmetry. The Weyl node W1 occurs at $(k(\frac{2\pi}{a}) = 0.2, 0.2, 0.2)$, 189 meV below E_F, while Weyl node W2 occurs at $(k(\frac{2\pi}{a}) = 0.167, 0.167, 0.167)$, 419 meV below E_F as shown in Fig. 2(c). These Weyl nodes are tilted and are of type-II character.[49,50] The corresponding Chern numbers are listed in Table I. The Weyl points act like "magnetic" monopoles in momentum space with their charge represented by the chirality. They are sources of the "Berry flux" similar to the magnetic flux.[3] The Berry flux/curvature is defined as $F = \nabla_k \times A$, where $A(k) = \sum_{n=1}^{N} \langle u_{nk} | \nabla_k | u_{nk} \rangle$ is the Berry connection and N is the number of occupied bands. Moreover, the total integral of the Berry curvature (Chern number) of a closed torus around a Weyl point (by Stokes theorem) equals the total "monopole charge" enclosed inside.[3,6] The topological stability of the Weyl node can be related to the Gauss law,

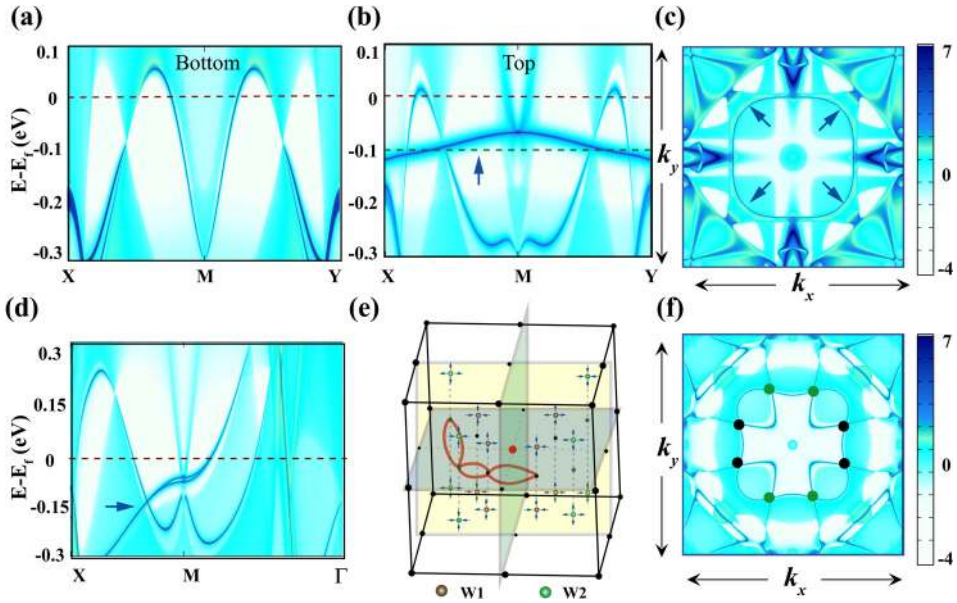

FIG. 3. Calculated (001) Bloch spectral function without SOC for (a) bottom and (b) top surface. The dark blue lines depict the surface state contribution. The surface states are more dispersive on the bottom surface than those on the top. (c) Fermi surface with the chemical potential of −0.1 eV [green dashed line in (b)]. The dark blue regions depict the surface state contribution with the blue arrows pointing towards the drumhead states. (d) Calculated (001) Bloch spectral function with SOC. The blue arrow points toward the surface states with a linearly dispersing Dirac cone. (e) A schematic of the positions of all the Weyl points (W1 and W2) in the Brillouin zone with their chirality as well as their projections on the (001) surface (blue plane). The red loops depict the surface Fermi arcs connecting the Weyl nodes of opposite chirality. (f) (001) Fermi surface of the material with SOC. The dark blue regions depict the surface states. The black (W1) and green (W2) dots denote the Weyl points. These Weyl nodes are connected by surface Fermi arcs, which uniquely form a closed loop in $CaSn_3$.

which requires invariance of the total flux inside a given surface. Therefore, the Weyl node can only vanish when it annihilates with another Weyl node with opposite chirality and should always come in pairs. The net charge of all the Weyl nodes inside a Brillouin zone should be zero.[51] Thus, to obtain chirality, the Berry curvature was calculated in the vicinity of Weyl nodes. Our calculations indeed show that each node has either a positive or negative sign of Berry curvature, thereby acting as either a source or a sink [Figs. 2(c) and 3(e)]. The symmetry of the crystal engenders eight pairs of Weyl nodes in the 3D Brillouin zone of $CaSn_3$. Furthermore, with SOC, the linear dispersion resembling the character of a Dirac semimetal around the BT point between the X-M and X-R directions [Fig. 2(a)] develops gaps of magnitudes 60 meV and 10 meV, respectively. Thus, these BT points are not topologically protected and are accidental band touching.

Another peculiar feature of a Weyl semimetal is the presence of surface Fermi arcs. They must start and end at the projection of two (or more) Weyl points with different "monopole charge," in the surface Brillouin zone. To see the existence of Fermi arcs, we calculated the (001) surface states in the presence of SOC [see Figs. 3(d) and 3(f)]. The black and green circles denote the Weyl points, the light blue and white regions represent the spectral weight of some additional bulk bands near the surface region, whereas the dark blue curves show the surface states. The surface band structure shows band crossing surface states with a linearly dispersing Dirac cone [Fig. 3(d)]. Moreover, Fermi arcs [Fig. 3(f)] appear in the surface spectrum connecting the Weyl nodes. The connectivity pattern of Fermi arcs in $CaSn_3$ is similar to the Weyl nodes observed in TaAs,[52] where a pair of Fermi arcs connects the Weyl nodes, instead of a just one. This peculiarity in the Fermi surface spectrum is observed because of the Weyl nodes of the same chiral charge from both top and bottom half of the Brillouin zone project at the same point on the (001) plane [Fig. 3(e)], thereby forming a closed loop of surface states. Moreover, the Weyl nodes with different chirality should be connected by Fermi arcs irrespective of whether they form a pair or not, as evident in this case also.

TABLE I. The coordinates, Chern numbers, and energies relative to the Fermi level of WPs of $CaSn_3$. Other WPs can be obtained by symmetry operations $\mathcal{I}$, $\mathcal{C}\,2_y$, and $\mathcal{C}\,2_z$.

Weyls points	Coordinates (k_x, k_y, k_z) $2\pi/a$	Chern number	$E - E_F$ (meV)
W_1	(0.20, 0.20, 0.20)	−1	189
W_2	(0.167, 0.167, 0.167)	+1	419

$CaSn_3$ is similar to other materials from the TaAs family[6] exhibiting nodal lines to Weyl semimetal evolution with SOC. Moreover, the SOC strength can be diminished in $CaSn_3$ by doping or substituting lighter elements such as Si or Ge in place of Sn. This will potentially allow a topological phase transition between the nodal-line semimetal and the Weyl semimetal. The details of this topological phase transition and interesting physics arising due to the synergy between the two phases with the tuning of SOC will be discussed in the future work. Moreover, materials hosting Weyl nodes have been found to show large negative magnetoresistance due to a chiral anomaly effect.[17–19] Thus, magnetoresistance experiments

can be done to verify our predictions in $CaSn_3$. However, the existence of Weyl nodes in centrosymmetric and time-reversal invariant superconducting $CaSn_3$ is intriguing and remains an open question.

IV. CONCLUSION

In summary, we have theoretically predicted a non-trivial band topology in a superconducting material—$CaSn_3$. This material has topological line nodes with drumhead surface states in the absence of SOC. The presence of SOC drives the material to the Weyl semimetallic state with surface Fermi arcs. The surface Fermi arcs are peculiar in $CaSn_3$; compared to other known Weyl Semimetals, these form closed loops of surface states on the Fermi surface. Moreover, unlike previously proposed topological superconductors, this material is intrinsically superconducting and does not require any external tuning such as doping and external pressure to drive superconductivity. In light of these unique properties, this material is expected to serve as an ideal platform for understanding the coupling between topological physics and superconductivity.

ACKNOWLEDGMENTS

The authors thank Dr. Swaminathan Venkataraman for valuable discussions. R.S. acknowledges the Science and Engineering Research Board, DST, India, for a fellowship (PDF/2015/000466). This work was partly supported by the U.S. Army Contract No. FA5209-16-P-0090. We also acknowledge the Materials Research Center and Supercomputer Education and Research Centre, Indian Institute of Science, for providing the required computational facilities.

[1]M. Z. Hasan and C. L. Kane, Rev. Mod. Phys. **82**, 3045 (2010).
[2]X.-L. Qi and S.-C. Zhang, Rev. Mod. Phys. **83**, 1057 (2011).
[3]X. Wan, A. M. Turner, A. Vishwanath, and S. Y. Savrasov, Phys. Rev. B **83**, 205101 (2011).
[4]H. Weyl, Z. Phys. **56**, 330 (1929).
[5]G. Bian, T.-R. Chang, R. Sankar, S.-Y. Xu, H. Zheng, T. Neupert, C.-K. Chiu, S.-M. Huang, G. Chang, I. Belopolski, D. S. Sanchez, M. Neupane, N. Alidoust, C. Liu, B. Wang, C.-C. Lee, H.-T. Jeng, C. Zhang, Z. Yuan, S. Jia, A. Bansil, F. Chou, H. Lin, and M. Z. Hasan, Nat. Commun. **7**, 10556 (2016).
[6]H. Weng, C. Fang, Z. Fang, B. A. Bernevig, and X. Dai, Phys. Rev. X **5**, 011029 (2015).
[7]S.-Y. Xu, I. Belopolski, N. Alidoust, M. Neupane, G. Bian, C. Zhang, R. Sankar, G. Chang, Z. Yuan, C.-C. Lee, S.-M. Huang, H. Zheng, J. Ma, D. S. Sanchez, B. Wang, A. Bansil, F. Chou, P. P. Shibayev, H. Lin, S. Jia, and M. Z. Hasan, Science **349**, 613 (2015).
[8]Z. Wang, Y. Sun, X.-Q. Chen, C. Franchini, G. Xu, H. Weng, X. Dai, and Z. Fang, Phys. Rev. B **85**, 195320 (2012).
[9]A. Burkov, M. Hook, and L. Balents, Phys. Rev. B **84**, 235126 (2011).
[10]M. Neupane, S.-Y. Xu, R. Sankar, N. Alidoust, G. Bian, C. Liu, I. Belopolski, T.-R. Chang, H.-T. Jeng, H. Lin, A. Bansil, F. Chou, and M. Z. Hasan, Nat. Commun. **5**, 3786 (2014).
[11]T. Liang, Q. Gibson, M. N. Ali, M. Liu, R. J. Cava, and N. P. Ong, Nat. Mater. **14**, 280 (2014).
[12]Y. Chen, Y. Xie, S. A. Yang, H. Pan, F. Zhang, M. L. Cohen, and S. Zhang, Nano Lett. **15**, 6974 (2015).
[13]B. Bradlyn, J. Cano, Z. Wang, M. G. Vergniory, C. Felser, R. J. Cava, and B. A. Bernevig, Science **353**, aaf5037 (2016).
[14]B. J. Wieder, Y. Kim, A. M. Rappe, and C. L. Kane, Phys. Rev. Lett. **116**, 186402 (2016).
[15]J. Nayak, S.-C. Wu, N. Kumar, C. Shekhar, S. Singh, J. Fink, E. E. D. Rienks, G. H. Fecher, S. S. P. Parkin, B. Yan, and C. Felser, Nat. Commun. **8**, 13942 (2017).
[16]C. Shekhar, A. K. Nayak, Y. Sun, M. Schmidt, M. Nicklas, I. Leermakers, U. Zeitler, Y. Skourski, J. Wosnitza, Z. Liu, Y. Chen, W. Schnelle, H. Borrmann, Y. Grin, C. Felser, and B. Yan, Nat. Phys. **11**, 645 (2015).
[17]A. Zyuzin and A. Burkov, Phys. Rev. B **86**, 115133 (2012).
[18]D. Son and B. Spivak, Phys. Rev. B **88**, 104412 (2013).
[19]C.-Z. Li, L.-X. Wang, H. Liu, J. Wang, Z.-M. Liao, and D.-P. Yu, Nat. Commun. **6**, 10137 (2015).
[20]L.-X. Wang, C.-Z. Li, D.-P. Yu, and Z.-M. Liao, Nat. Commun. **7**, 10769 (2016).
[21]T. Grover, D. Sheng, and A. Vishwanath, Science **344**, 280 (2014).
[22]S. Sasaki and T. Mizushima, Physica C **514**, 206 (2015).
[23]S. A. Yang, H. Pan, and F. Zhang, Phys. Rev. Lett. **113**, 046401 (2014).
[24]S.-Y. Xu, N. Alidoust, I. Belopolski, A. Richardella, C. Liu, M. Neupane, G. Bian, S.-H. Huang, R. Sankar, C. Fang, B. Dellabetta, W. Dai, Q. Li, M. J. Gilbert, F. Chou, N. Samarth, and M. Z. Hasan, Nat. Phys. **10**, 943 (2014).
[25]Y. S. Hor, A. J. Williams, J. G. Checkelsky, P. Roushan, J. Seo, Q. Xu, H. W. Zandbergen, A. Yazdani, N. P. Ong, and R. J. Cava, Phys. Rev. Lett. **104**, 057001 (2010).
[26]T. Sato, Y. Tanaka, K. Nakayama, S. Souma, T. Takahashi, S. Sasaki, Z. Ren, A. A. Taskin, K. Segawa, and Y. Ando, Phys. Rev. Lett. **110**, 206804 (2013).
[27]R. D. Zhong, J. A. Schneeloch, T. S. Liu, F. E. Camino, J. M. Tranquada, and G. D. Gu, Phys. Rev. B **90**, 020505 (2014).
[28]Y. Qi, P. G. Naumov, M. N. Ali, C. R. Rajamathi, W. Schnelle, O. Barkalov, M. Hanfland, S.-C. Wu, C. Shekhar, Y. Sun, V. Süß, M. Schmidt, U. Schwarz, E. Pippel, P. Werner, R. Hillebrand, T. Förster, E. Kampert, S. Parkin, R. J. Cava, C. Felser, B. Yan, and S. A. Medvedev, Nat. Commun. **7**, 11038 (2016).
[29]L. Fu and C. L. Kane, Phys. Rev. Lett. **100**, 096407 (2008).
[30]X. Luo, D. F. Shao, Q. L. Pei, J. Y. Song, L. Hu, Y. Y. Han, X. B. Zhu, W. H. Song, W. J. Lu, and Y. P. Sun, J. Mater. Chem. C **3**, 11432 (2015).
[31]W. Kohn and L. J. Sham, Phys. Rev. **140**, A1133 (1965).
[32]G. Kresse and J. Furthmüller, Comput. Mater. Sci. **6**, 15 (1996).
[33]G. Kresse and J. Furthmüller, Phys. Rev. B **54**, 11169 (1996).
[34]P. E. Blöchl, Phys. Rev. B **50**, 17953 (1994).
[35]G. Kresse and D. Joubert, Phys. Rev. B **59**, 1758 (1999).
[36]J. P. Perdew, K. Burke, and M. Ernzerhof, Phys. Rev. Lett. **77**, 3865 (1996).
[37]H. J. Monkhorst and J. D. Pack, Phys. Rev. B **13**, 5188 (1976).
[38]A. A. Mostofi, J. R. Yates, G. Pizzi, Y.-S. Lee, I. Souza, D. Vanderbilt, and N. Marzari, Comput. Phys. Commun. **185**, 2309 (2014).
[39]M. L. Sancho, J. L. Sancho, J. L. Sancho, and J. Rubio, J. Phys. F: Met. Phys. **15**, 851 (1985).
[40]W. QuanSheng and Z. ShengNan, see https://github.com/quanshengwu/wannier_tools for WannierTools code, a tool for the investigation of novel topological materials.
[41]H. Huang, J. Liu, D. Vanderbilt, and W. Duan, Phys. Rev. B **93**, 201114 (2016).
[42]R. Yu, H. Weng, Z. Fang, X. Dai, and X. Hu, Phys. Rev. Lett. **115**, 036807 (2015).
[43]I. Y. Sklyadneva, I. P. Rusinov, R. Heid, K.-P. Bohnen, P. M. Echenique, and E. V. Chulkov, Sci. Rep. **6**, 24137 (2016).
[44]Y.-H. Chan, C.-K. Chiu, M. Y. Chou, and A. P. Schnyder, Phys. Rev. B **93**, 205132 (2016).
[45]H. Weng, Y. Liang, Q. Xu, R. Yu, Z. Fang, X. Dai, and Y. Kawazoe, Phys. Rev. B **92**, 045108 (2015).
[46]G. Bian, T.-R. Chang, H. Zheng, S. Velury, S.-Y. Xu, T. Neupert, C.-K. Chiu, S.-M. Huang, D. S. Sanchez, I. Belopolski, N. Alidoust, P.-J. Chen, G. Chang, A. Bansil, H.-T. Jeng, H. Lin, and M. Z. Hasan, Phys. Rev. B **93**, 121113 (2016).
[47]D. Vanderbilt and R. D. King-Smith, Phys. Rev. B **48**, 4442 (1993).
[48]A. Yamakage, Y. Yamakawa, Y. Tanaka, and Y. Okamoto, J. Phys. Soc. Jpn. **85**, 013708 (2015).
[49]Y. Xu, F. Zhang, and C. Zhang, Phys. Rev. Lett. **115**, 265304 (2015).
[50]A. A. Soluyanov, D. Gresch, Z. Wang, Q. Wu, M. Troyer, X. Dai, and B. A. Bernevig, Nature **527**, 495 (2015).
[51]H. B. Nielsen and M. Ninomiya, Phys. Lett. B **105**, 219 (1981).
[52]S.-M. Huang, S.-Y. Xu, I. Belopolski, C.-C. Lee, G. Chang, B. Wang, N. Alidoust, G. Bian, M. Neupane, C. Zhang, S. Jia, A. Bansil, H. Lin, and M. Z. Hasan, Nat. Commun. **6**, 7373 (2015).